Analyst

Accepted Manuscript

ROYAL SOCIETY OF CHEMISTRY

www.rsc.org/analyst

Journal Name

RSCPublishing

ARTICLE

Dip-Pen Microarraying of Molecular Beacon Probes on Microgel Thin-Film Substrates

Cite this: DOI: 10.1039/xoxxoooooox

Xiaoguang Dai and Matthew Libera[a]

Received ooth January 2012,
Accepted ooth January 2012

DOI: 10.1039/xoxxoooooox

www.rsc.org/

The integration of microarray-based nucleic acid detection technologies and microfluidics is attractive, because the combination of small sample volumes, relatively short diffusion distances, and solid-phase detection enhances the development of multiplexed assays with improved sensitivity and minimal sample size. However, traditional microarray spotting methods typically create probe spot sizes of ~50-100 μm diameter, comparable to the dimensions of many microfluidic channels. In addition, detection of hybridization events typically requires a post-hybridization labeling step. We address both issues by exploring the use of dip-pen nanolithography (DPN) to pattern linear oligonucleotides and self-reporting molecular beacon (MB) probes on streptavidin-functionalized poly(ethylene glycol) microgel thin-film substrates. In contrast to many systems involving DPN deposition, the fluorescence of the labeled probes enables their amount and spatial distribution to be characterized by optical microscopy. Their deposition rate decreases with increasing DPN dwell time, consistent with a Langmuir adsorption model, but the linear relationship between spot diameter and time$^{1/2}$ indicates that spot size is diffusion controlled. We then use DPN to pattern MB probes for the *mecA* and *spa* genes in *Staphylococcus aureus* as a 2-column array with 1 μm spot sizes and 5 μm spot spacings, and we use this array to differentiate targets characteristic of methicillin-resistant *S. aureus* (MRSA) and methicillin-sensitive *S. aureus*. This duplexed self-reporting gel-tethered MB microarray not only shows high specificity but also a high signal-to-background ratio.

Introduction

The effective treatment of a systemic or local infection requires microbial identification in order to prescribe an appropriate antimicrobial treatment. The traditional diagnosis approach cultures blood, sputum, urine, washes, swabs, or other bodily fluids to determine if microbes are present and then examines phenotypes within the culture, such as morphology or antimicrobial susceptibility, for identification. This approach often requires periods as long as 3-5 days to complete, during which time the prescription of antibiotics is under-informed and fraught with problems including serious threats to patient well-being. Molecular diagnostics (MDx) have radically changed the process of clinical microbial identification.[1-3] Importantly, MDx approaches are both specific and fast. Based on nucleic-acid hybridization methods, they can identify microbes to the species and strain level using biospecific markers and do so over a time scale that can be as short as one hour. Despite their effectiveness, however, MDx tests have not yet achieved widespread clinical use. The slower process of culturing and phenotyping remains standard. Among the reasons is that the throughput associated with MDx techniques is relatively low. Throughput - the number of tests that can be run within a given time period - is in part compromised by the complexity, and the cost, associated with target amplification, the nature and extent of multiplexing, and the detection. There have thus been increasing efforts to miniaturize and simplify these MDx platforms by exploiting microarray and lab-on-a-chip type formats that have the potential to simplify and integrate many of these functions and do so using a small footprint.[4-6]

Microarrays to probe DNA or RNA targets have traditionally been created by spotting probe oligonucleotides onto a substrate, which is often some form of surface-functionalized glass. This technology is well established.[7] Droplets of liquid solution containing capture probes are deposited onto the surface, whereupon the probes adhere to functional sites on the underlying surface either by physisorption or by covalent grafting. This approach typically produces spot diameters on the order of 50-100 μm or more. These length scales are on the same order as typical channel widths in many microfluidic devices, and even smaller feature sizes would further exploit the smaller sample volume and enhanced diffusion and transport associated with miniaturization.[8] Dip-pen nanolithography (DPN) is an alternate method for functionalizing surfaces with feature sizes of order 0.1-10 μm. While it initially was used primarily to pattern thiols on metal surfaces,[9, 10] its use has more recently been broadened to a broad variety of surface chemistries, patterning molecules, including DNA,[11-15] and applications including microarrays.[16-20]

Independent of how they are fabricated, the majority of DNA microarrays use linear oligonucleotides as the capture probes. These typically require some form of post-hybridization labeling in order to visualize them by a fluorescence imaging method. Molecular beacon (MB) probes, on the other hand, are self-reporting. They fluoresce when they hybridize to their complimentary targets.[21] While MB probes have been used extensively in solution-based assays, they have had substantially less success in a microarray format,[22, 23] because interactions with a hard substrate lead to an increased background, a decreased signal-to-background ratio, and thus to a reduced sensitivity. We recently were able to both immobilize MB probes at discrete locations on a solid substrate and preserve a high signal-to-background ratio by tethering the MB probes to highly hydrated microgels grafted to solid substrates by electron-beam patterning of biotinylated poly(ethylene glycol) (B-PEG).[24] Because of the microgel tethering, these probes are not in contact with the underlying hard substrate, and they reside in as water-like an environment as possible. Hence, their performance is much closer to that observed when they are untethered and free in solution. Importantly, surface tethering removes the requirement imposed by solution-based assays that different MB probes be functionalized with different fluorophores, since on a surface a specific MB probe can be identified based on its position rather than by its color. Microgel-tethered MB probes thus lend themselves well to a microarray format. However, combining microarray and lab-on-a-chip formats for MDx assays requires that individual spots in the array be functionalized with different probe molecules and that these spots be small enough to effectively work with small sample volumes within a microfluidic device.

Here we create a simple microscale nucleic acid hybridization array using DPN as a microscale spotting system to pattern biotinylated linear oligonucleotides and MB probes on streptavidin (SAv)-functionalized B-PEG microgel thin films. Significantly, these fluorescently labeled oligonucleotide probes enable us to characterize the amount of deposited probe and their spatial distribution by optical microscopy. We use this property to show that the oligonucleotide-binding rate near the point of AFM incidence is consistent with a Langmuir adsorption model but that the overall spot diameter is controlled by diffusion. This finding suggests that a binding event occurs much less frequently than an increment of diffusive motion. To demonstrate the utility of this approach, we use DPN to create a simple duplex array with four-fold redundancy, appropriate for detecting for staph infection. The 2 x 4 array occupies an area of less than 150 μm^2 and exhibits both high specificity and a high signal-to-background ratio.

Results and discussion

1. Microgel thin-film fabrication

Microgel thin films were created using electron-beam lithography with B-PEG as the resist polymer (Figure 1). B-PEG thin films, about 60 nm thick, were solvent cast from 2 wt% tetrahydrofuran (THF) solutions. After drying the films were exposed to a focused beam of 2 keV electrons, which both crosslink the PEG and graft it to the underlying plasma-treated silicon substrate. The inter-pixel distance (200 nm) was close enough so that the resulting microgels produced by each point irradiation overlapped to create a continuous microgel thin film. After washing in a good solvents (methanol), to remove unexposed B-PEG, the microgels were then immersed in a SAv solution to enable the subsequent binding of biotinylated linear oligonucleotides or biotinylated MBs.

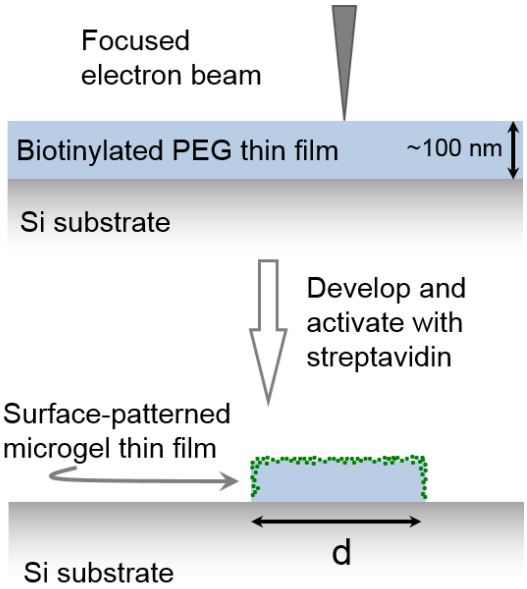

Figure 1. Biotinylated PEG (B-EPG) is spin-coated onto plasma-treated Si and crosslinked using energy from a focused electron beam. After removing unexposed B-PEG by washing in methanol (develop), the B-PEG microgel thin film is activated by exposure to streptavidin. The lateral size of the microgel film can be controlled from sub-micron to millimeter length scales.

Despite the fact that the PEG microgel film is highly hydrophilic, water contact-angle measurements show that the surface wetting properties depend on the nature of the terminal groups on the PEG. For example, the water contact angle of the as-patterned B-PEG microgel thin film is 19.7 ±0.3 (the average and standard deviation for n=3). After exposure to SAv the contact angle increases to 23.4 ± 0.3. In contrast, comparable films formed from hydroxyl-terminated PEG (OH-PEG) exhibit a contact angle of 14.3 ±0.4. The larger contact angle of the SAv-covered microgel thin film may be in part due to the fact that that the hydrophilic PEG chains on the surface are partially shielded from the surrounding water by SAv-biotin conjugates.

2. Homogeneous oligonucleotide conjugation

In contrast to common hard substrates such as silicon or glass, with or without a metal coating (e.g. gold), a PEG microgel film is a soft and hydrophilic polymer network, and assessing the size, shape, and extent of functionalization within a spot of deposited DNA by topographic or lateral force AFM is difficult. Instead, we used fluorescence optical microscopy.[25] Although this approach suffers from lower resolution, unlike topographic and lateral-force AFM, the image contrast (fluorescence intensity) gives information about the number of bound oligonucleotide ink molecules.

To understand the relationship between the measured fluorescence intensity and the number of bound fluorophores, we performed a control experiment where a silicon wafer patterned with SAv-activated B-PEG microgel thin film pads was immersed in an aqueous solution of *mecA* linear oligonucleotide probe (L-probe). Figure 2A shows a fluorescence image of five such pads. Each pad is made up of an array of individual microgels, and the number of microgels in each pad increases as

the pad diameter increases. Because the binding reaction occurs in solution, the *mecA* L-probes cover the microgels homogenously. A one-hour reaction time also ensures that the microgel binding sites are fully saturated by L-probe. There is a linear relationship between the total fluorescence intensity from each of the five thin-film pads and the number of microgels within each pad (Figure 2B). The inset to Figure 2B is a line profile of fluorescence intensity, averaged over a two-pixel width, of three microgel pads. These profiles correspond to the convolution of the *mecA* L-probe spatial distribution (object) on the surface and the point spread function (PSF) of the microscope. The object is illustrated as a top-hat intensity distribution because the L-probes are immobilized homogeneously on the microgel pad and the concentration of SAv binding sites drops to zero abruptly at the edge of each pad. The PSF of the 2D wide-field fluorescence microscope (NA = 0.8, λ_{em} = 595 nm) can be approximated by a Gaussian function, where $\sigma = 0.21\frac{\lambda_{em}}{NA} = 156nm$.[26]

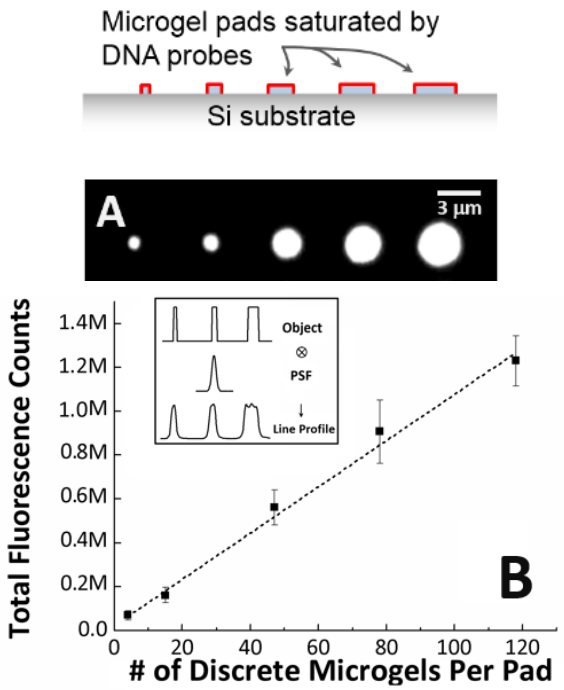

Figure 2. (A) Electron-beam patterned, SAv-activated PEG microgel thin-film pads with different lateral sizes are saturated homogeneously by immersion into a solution of Texas Red-labeled *mecA* L-probe. The microgel pad diameters are 0.5, 1, 1.5, 2 and 2.5 μm; (B) The total fluorescence intensity per pad is proportional to the number of individual microgels contained within each microgel pad. The errors bars are the standard deviations of three different measurements. The line profile in the inset is extracted from the 0.5, 1 and 1.5 μm spots and corresponds to the convolution of the microscope point spread function (PSF) and the actual *mecA* L-probe distribution on the microgel pads (object).

3. Humidity effects

When exposed to humidity or immersed in an aqueous solution, the PEG microgel films swell and do so primarily in the direction perpendicular to the underlying Si surface.[27, 28] We used AFM to measure the heights of SAv-activated B-PEG microgel films at relative humidities (RHs) of 35%, 50%, 65% and 80%. The average and standard deviation from three measurements measured at each humidity are: 64.6 ±2.8; 59.5 ± 2.1; 61.5 ± 5.0; and 122.8 ± 17.4, respectively. The average microgel film height almost doubles as the RH increases from 65% to 80%. We attribute this behavior to the absorption of atmospheric water into the gel, which causes the crosslinked polymer network to swell. A thickness of 123 nm at 80% RH is about the same as that observed when the same microgel thin film is fully saturated by immersion in deionized (DI) water. We furthermore find that reproducible DPN patterning of oligonucleotides on the microgel thin-film substrates can only be achieved with RH > 75%, suggesting that above RH = 75% the internal polymer network is saturated by water and is thus able to contribute water to the meniscus when an AFM tip contacts the substrate. We confirmed that a meniscus forms by making AFM force-displacement measurements[29] at RH = 80% where we observe a strong pull-off force. Topographic AFM imaging after pull-off shows that the AFM tip penetrates the hydrated soft polymer network, which during DPN brings the oligonucleotides on the tip apex in direct contact with the surrounding microgel film.

4. Oligonucleotide micropatterning

In order to visualize the patterned oligonucleotides in the absence of target hybridization, we first used the *mecA* L-probe as an ink. Figure 3A presents a representative fluorescence image showing four spots of Texas-Red-labeled *mecA* L-probe patterned on a continuous SAv-activated B-PEG microgel film. From left to right the DPN dwell times are 0.5, 2, 8, and 16 s. Figure 3B shows line profiles, averaged over a two-pixel width, of the fluorescence intensity from each spot. Figures 3A and 3B indicate that the peak intensity and lateral size of the DNA oligonucleotide spots are both related to dwell time.

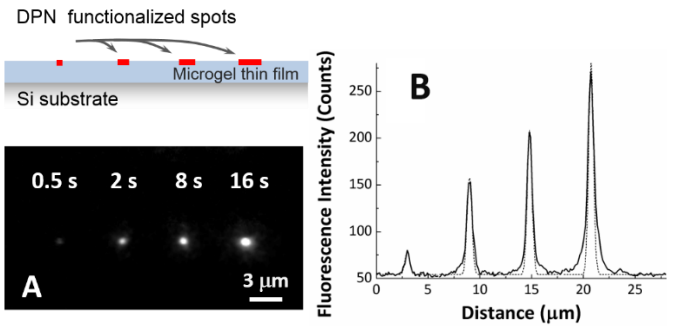

Figure 3. (A) Fluorescence microscope image of DPN spots of Texas Red-labeled *mecA* L-probe on a continuous SAv-activated B-PEG microgel thin-film substrate. The DPN dwell times are 0.5, 2, 8 and 16 s (left to right); (B) Intensity profiles (2 pixel width) over the four DPN spots. The peak intensities and spot sizes both depend on dwell time. The dotted lines are Gaussians with a standard deviation determined by fitting to the 0.5 s intensity profile.

4.1 Binding near the incident point

As the dwell time increases from 0.5 to 16 s, the four peak intensities, after background subtraction, also increase. However, their magnitudes (Figure 3B) vary from only 1.3% to 11.8% of the intensity in the fully saturated control experiment (Figure 2). This low but growing peak intensity indicates that the surface density of immobilized *mecA* L-probes around the incident point continuously increases while the AFM tip is in contact with the microgel thin film. Such behavior is different from that observed in many DPN experiments where AFM imaging of bound ink molecules indicates that a uniform SAM forms around the incident point and ink binding only occurs on the edge of the growing SAM.[15, 30, 31]

To study DNA binding around the point where the inked AFM tip touches the substrate, we define a near-incident point (NIP) region as the Full Width at Tenth Maximum (FWTM) of the Gaussian fit to the line profile of the 0.5 s spot. In Figure 3B, the four Gaussian functions (dotted lines) have the same FWTM. We extracted the total fluorescence intensity in the four NIP regions and plot these as a function of dwell time in Figure 4.

In contrast to the amphiphilic or insoluble DPN inks such as 16-mercaptohexanoic acid (MHA) or octadecanethiol (ODT), oligonucleotides are charged and water soluble. Consequently, a bulk transport process should be used to model DNA patterning through the meniscus.[32, 33] We model the oligonucleotide binding

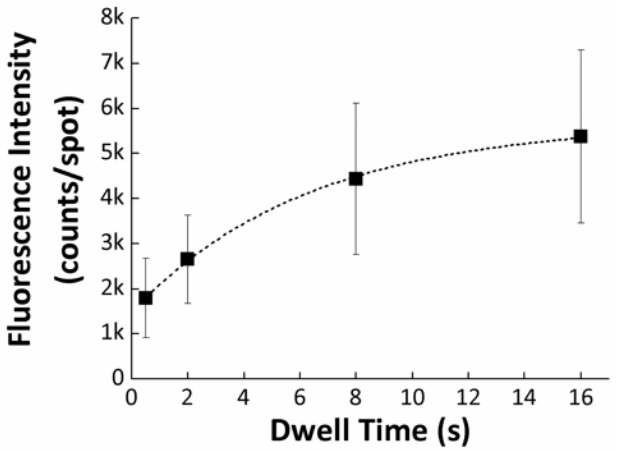

Figure 4. The integrated fluorescence intensity characteristic of the near-incidence point region in each spot increases with increasing DPN dwell time and follows a Langmuir adsorption model (dotted line). The points and the error bars are the average and the standard deviation, respectively, of at least 15 independent measurements.

in the NIP region using a Langmuir adsorption approach. The binding rate can be described by:

$$\frac{d\Gamma(t)}{dt} = k_a C_e (1 - \frac{\Gamma(t)}{\Gamma_{max}}) \quad (1)$$

Where $\Gamma_{(t)}$ is the time-dependent density of occupied surface binding sites, Γ_{max} is the maximum density of binding sites, C_e is the oligonucleotide concentration in the meniscus, t is time, and k_a is the association constant. Solving eq. (1) gives:

$$\Gamma(t) = \Gamma_{max} - C_1 e^{-k_a C_e t / \Gamma_{max}} \quad (2)$$

As shown in Figure 4, this first-order exponential decay fits the extracted fluorescence intensity per spot data well (dotted line). Since $\Gamma_{(t=0)} \neq 0$, the constant C_1 is not equal to Γ_{max}, suggesting a non-zero initial adsorption. We attribute this behavior to the fact that the soft PEG microgel film is indented by, and thus partially in contact with, the apex of the AFM tip during spotting. In immediate proximity to the tip in this indented region, the initial oligonucleotide-binding rate could consequently be faster and largely dominated by a process similar to microcontact printing.

The Langmuir model indicates that the oligonucleotide-binding rate in the present experiments is determined by the fraction of available binding sites on the microgel thin-film surface. This suggests that: (i) the oligonucleotides can easily detach from the AFM tip; (ii) the meniscus in the NIP region is fully saturated with oligonucleotide C_e is the solubility of the oligonucleotides in solution); and (iii) the size of the meniscus is small relative to the diffusion distance of the oligonucleotide. These are all reasonable properties. The oligonucleotide solubility in water is relatively high, and the bulk diffusivity of the 35-base *mecA* L-probe is about 3×10^{-7} cm^2 s^{-1} in DI water,[34] so that it can diffuse several microns or more in 0.5 s. Note that the longest dwell time in our experiment is only 16 s, and, we used inked tips for over 15 repetitions of patterning without noticing reductions in fluorescence intensities, indicating that the decrease in binding rate with increasing dwell time is not due to the depletion of ink molecules from the AFM tip.[35-37]

4.2 Time-Dependent Spot Size

The FWTM of the Gaussians in Figure 3B, which defines the NIP regions, is 1.0 μm. The fluorescence line profiles in this region follow Gaussians because of the convoluting effects of the Gaussian PSF of the microscope. Surrounding the NIP region is a corona that has lower fluorescence intensity. This is especially evident for longer dwell times where the corona was repeatedly observed and extended as much as 2-3 μm from the spot center. We determined the spot diameters for dwell times of 0.5, 2, 8 and 16 s from fifteen independent experimental data sets. In each case, we defined the edge of a DPN spot as the point where the signal falls to a value corresponding to the average background plus three times the standard deviation of that background. The result is plotted in Figure 5, and it shows that the spot radius (r) follows a linear relationship with the square root of dwell time suggesting that the oligonucleotides follow 2D Fickian diffusion in the corona region.[32, 38]

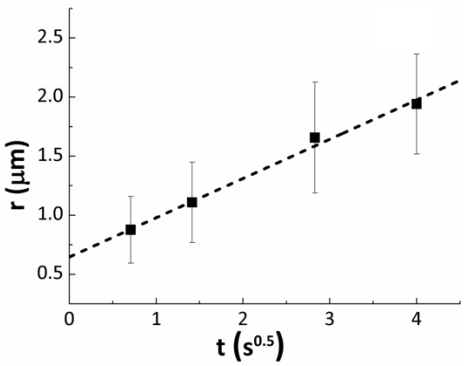

Figure 5. The radii of DPN spotted *mecA* L-probe increases linearly with the square root of time. The points and the error bars are the average and standard deviation, respectively, of at least 15 independent measurements.

A linear dependence of DPN spot radius on the square root of dwell time has been observed previously in a number of DPN studies.[30, 33, 38] In the case of model studies involving alkane thiols, this behavior has been attributed to the diffusion of ink molecules across the surface of a previously deposited self-assembled monolayer followed by binding to the substrate at the

edge of the SAM where the ink concentration drops abruptly to zero and there is essentially a continuum of binding sites offered by the underlying metal surface. The situation in the case of biotinylated oligonucleotides diffusing across a streptavidin-activated B-PEG microgel thin film is somewhat different. We know from previous measurements[24] that the binding sites on SAv-activated B-PEG microgels, made from pure 5 kDa B-PEG, are separated from each other by distances of about 5 nm. Outside the near-incidence region, the biotinylated oligonucleotides are thus diffusing across a surface with a heterogeneous distribution of binding sites. The fact that the oligonucleotides continue to diffuse radially outward despite the presence of a large population of unoccupied bind sites suggests that the characteristic time scale for a diffusive jump is shorter than that for a binding event. This presumably is related to the fact that the biotin is located at one end of each oligonucleotide (Table 1), and binding requires both proper positioning as well as proper orientation relative to an underlying SAv.

5. Multiplexed microarray of molecular beacon probes

Having established conditions for oligonucleotide patterning on microgel thin film substrates, we used DPN to create microspots of *mecA* and *spa* MBs in a 2 x 4 array format (Figure 6) using a 2 s DPN dwell time. Because the *spa* gene exists in all *S. aureus* and the *mecA* gene only exists in the strain of methicillin-resistant *S. aureus* (MRSA), a positive signal from a *spa* MB indicates that a target is *S. aureus*, and a positive signal from a *mecA* MB further indicates that the target is MRSA. The sequences of *mecA*/*spa* MBs and their complementary targets are listed in Table 1. While here we use only two different MB probes, the multiplexity of such a DPN-patterned MB array can in principle be much higher.

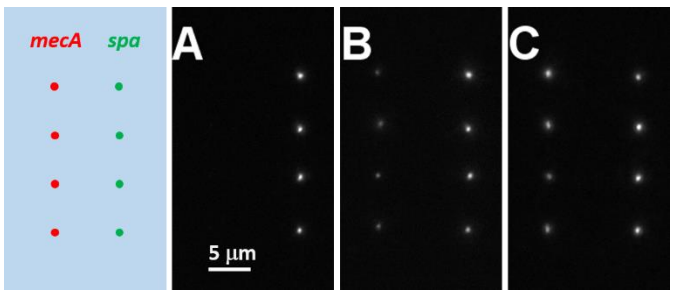

Figure 6. A 2 x 4 array of DPN-patterned spots of *mecA* (left row) and *spa* (right row). The three right images show: (A) MB probes after incubation in a 10^{-6} M *spa* target solution; (B) the sample from (A) after washing and subsequent incubation in a 10^{-6} M *mecA* target solution; and (C) a different 2 x 4 array after incubation in a binary mixture of 10^{-6} M *mecA*/*spa* targets.

Figure 6A shows a fluorescence microscope image taken after the 2 x 4 bifunctional MB probe array was exposed for 30 min to a 10^{-6} M *spa* target solution in PBS. Only the 4 *spa* MB spots fluoresce (right row). Following this imaging step, the array was washed with PBS and immersed in *mecA* target solution for another 30 min. As a result, the *mecA* MB spots (left row) also fluoresce (Figure 6B) while the *spa* MBs remain hybridized (right row). A different 2 x 4 bifunctional array was exposed to a binary mixture of both *mecA* and *spa* targets, and, as shown in Figure 6C, both of the 4 *mecA* MB (left) spots and the 4 *spa* MB (right) spots fluoresce. The importance of such a multiplexed MB array lies in its self-reporting property and micron-scale feature size for possible applications in digitized droplet analysis with sample volumes at the picoliter level when integrated with microfluidic devices.

To quantify the extent to which the performance of the MBs is retained during the patterning and hybridization processes, we calculated the signal-to-background ratio by comparing the fluorescence intensity of the *mecA* MB spots in Figure 6B (background) and 6C (signal) as defined previously.[24] The four DPN *mecA* MB spots demonstrate an average signal-to-background ratio of 19.7. While still substantially less than that observed by control experiments involving the hybridization of untethered *mecA* and *spa* MBs in solution,[24] this value is nevertheless higher than that of most surface-immobilized MBs, which typically range from 5-10 or less.[22, 23, 39] However, 19.7 is significantly lower than what we previously observed using buffer-based immobilization (signal-to-background ratio~45-60) rather than DPN immobilization.[24] This difference is at least in part due to the fact that the DPN approach of patterning biotinylated oligonucleotides on a SAv-activated PEG microgel thin film does not fully saturate the available SAv binding, so the signal is lower than that observed when immobilizing from buffer.

Table 1. Sequences of Molecular Beacon probes and oligonucleotides used.[a]

Oligos	Sequence (5'–3')
mecA MB	TexasRed_CGCGATTTCAATATGTATGCTTTGGTCTT TCTGCATCGCG-dT-BHQ2-TEG-biotin
spa MB	TexasRed_CGCGACTTGTTGAGCTTCATCGTGTTGCG CGTCGCG-dT-BHQ2-TEG-biotin
mecA L-probe	TexasRed_CGCGATTTCAATATGTATGCTTTGGTCTT TCTGCA-TEG-Biotin
mecA target	CCAGGAATGCAGAAAGACCAAAGCATACATATTG AAAATTTAAA
spa target	GCAAATGCTGCGCAACACGATGAAGCTCAACAAA ATGCTTTTTA

[a] The underlined portions indicate the probing regions.

Experimental

Materials 5 mm x 7 mm silicon wafers were purchased from Ted Pella (Redding, CA). Biotin-PEG-Biotin (B-PEG, M_w = 5 kDa) was purchased from Nanocs Inc. (New York, NY). M-type AFM tips used for DPN were purchased from NanoInk Inc. (Skokie, IL). 3-aminopropyltrimethoxysilane (APTMS) was purchased from Gelest (Morrisville, PA). *mecA* L-probe and all the targets were purchased from Integrated DNA Technologies (IDT, Coralville, Iowa). MB probes were synthesized at the Public Health Research Institute (PHRI, Newark, NJ) using standard automatic DNA chemistry on an ABI 394 DNA/RNA synthesizer (Applied Biosystems, Foster, CA). H_2O_2 (30%), SAv and PBS were purchased from Thermo Scientific (Rockford, IL).

Sulfuric acid (95-98%), tetrahydrofuran (99.8%), methanol (99.8%), Tween-20, $MgCl_2$ solution (1 M) and toluene (anhydrous, 99.8%) were purchased from SigmaAldrich (St. Louis, MO). All chemicals were used as received.

Fabrication of biotinylated-PEG microgel thin film Electron-beam patterned PEG microgel thin films were prepared following procedures described previously[28] using a Zeiss Auriga FIB-SEM CrossBeam Microscope equipped with a Nanometer Pattern Generation System (NPGS, Nabity, Bozeman, MT). 5 μm × 5 μm patches of pseudo-continuous B-PEG microgel films were fabricated using an inter-gel spacing of 200 nm and a point dose of 10 fC with 2 keV electrons. Prior to DPN, the patterned microgels were activated by immersion in a SAv solution (200 μg mL^{-1}, 100 mM Na_3PO_4, 150 mM NaCl, pH 7.4) for 1 hour. Unreacted SAv solution was removed by a washing buffer (0.05% Tween-20, 100 mM Na_3PO_4, 150 mM NaCl). The entire wafer was then carefully dried by gentle centrifugation. The static wetting angles were examined at ambient condition using a contact angle goniometer (Model 500, Ramé-Hart, Succasunna, NJ).). Note that, because of how focused electron irradiation deposits energy into the B-PEG thin-film precursor, the patterned microgels and microgel thin films exhibit a crosslink density that is very high within the microgel and very low at the microgel surface.[24] Consequently, SAv and oligonucleotide binding is localized at and near the microgel/water interface.

Dip-pen nanolithography DPN was carried out on using an Nscriptor DPN system (NanoInk Inc.). Inks involving either biotinylated, Texas Red-labeled, linear oligonucleotide (L-probe) or MB probes (Table 1)[24] were created by dissolving the oligonucleotides in a buffer solution (5 mg mL^{-1} PEG (M_w = 6 kDa), 100 mM Na_3PO_4 and 150 mM NaCl, pH 5) at a concentration of 8 μM. Ink solution was pipetted into multi-channel inkwells (NanoInk Inc.), and the L-probes or MBs were adsorbed onto APTMS-coated M-2 AFM tips (k = 0.6 N m^{-1}) by immersing the tips in the micro channels for 5 min. The oligonucleotides were negatively charged at pH 5. The silanol groups on the tip were neutralized by H^+, and the amine groups from the APTMS layer on the tips were positively charged. Therefore, the adsorption of oligonucleotides to the tip was driven by a strong electrostatic interaction.[40] After removal from an inkwell, the ink remaining on the AFM tip was dried by exposure to gently flowing nitrogen gas. The tip was then warmed to 50 °C and held there for 20 min. Unless otherwise noted, DPN patterning was conducted at a relative humidity of 75% - 80% and a temperature of 24 °C. During patterning, the tips were kept in contact with the substrate by laser reflection feedback control with an applied force of 200 nN.

Hybridization Experiments Hybridization experiments were carried out by immersing the DPN-patterned 2-column MB microarrays on microgel thin-films in a hybridization buffer (4 mM $MgCl_2$, 50 mM KCl, 10 mM Tris-HCl, pH 8.0) containing complementary *mecA* or (and) *spa* targets (1 μM, Table 1) for 30 min in a humid atmosphere. Fluorescence images were taken directly after hybridization without any washing steps.

Imaging Fluorescence images were taken at room temperature using a Nikon E1000 upright fluorescence microscope with a SensiCam high-sensitivity CCD Camera (Cooke, PCO-TECH Inc.) and a 50x objective lens (LU PLAN, NA = 0.8). The exposure time was 4 s for all images. Topographical AFM images were collected in non-contact mode with a scanning speed of 5 μm s^{-1} using the Nscriptor DPN system operated in imaging mode.

Conclusions

We have explored using DPN as a microspotting method to create microscale arrays of self-reporting MB probes for possible application in molecular diagnostic detection technologies. Importantly, the substrate consists of a microgel thin film, which not only introduces an important tethering environment for immobilizing the oligonucleotide probes but also brings a soft and highly hydrated substrate with a heterogenous distribution of surface binding sites on which to do DPN. Significantly, these fluorescently labeled oligonucleotide probes enable us to characterize the amount of deposited probes and their spatial distribution by optical microscopy. Near the point where the inked AFM tip contacts the microgel film, the oligonucleotide-binding rate decreases with increasing dwell time but, consistent with a Langmuir adsorption model, the biotinylated oligonucleotides do not saturate the available SAv binding sites on the microgel thin-film surface. The linear relationship between overall spot diameter and time$^{1/2}$ nevertheless suggests that spot size is controlled by oligonucleotide diffusion away from the AFM tip. In contrast to traditional spotting techniques, which produce relatively large (~50-100 μm) spots separated from each other by relatively large distances, DPN can create micron-size spots in very close proximity to each other. We pattern two different molecular beacons, which probe the *mecA* and *spa* genes in *S. aureus*, onto PEG microgel substrates as a 2-column microarray, with micron-sized spots separated from each other by ~ 5 μm, and use this array to differentiate targets characteristic of MRSA from methicillin sensitive *S. aureus*. This duplexed self-reporting microarray shows both high specificity and a high signal-to-background ratio. The size, scalability, and success of this array suggest that it may be useful in lab-on-a-chip type applications for the rapid detection of infection and other clinically relevant molecular diagnostic applications.

Acknowledgements

The authors would like to thank Dr. Salvatore Marras of the Public Health Research Institute (Newark, NJ) for his early involvement in this research activity. This project was supported by the U.S. Army Research Office via grant #W911NF-12-1-0331.

Notes and references

[a] Department of Chemical Engineering and Materials Science
Stevens Institute of Technology
Castle Point on Hudson, Hoboken, New Jersey 07030, United States

1. A. Deshpande and P. S. White, *Expert Rev Mol Diagn*, 2012, **12**, 645-659.
2. B. C. Millar, J. Xu and J. E. Moore, *Current Issues in Molecular Biology*, 2007, **9**, 21-40.
3. K. L. Muldrew, *Current Opinion in Pediatrics*, 2009, **21**, 102-111.
4. K. Y. Lien and G. B. Lee, *Analyst*, 2010, **135**, 1499-1518.
5. C. Situma, M. Hashimoto and S. A. Soper, *Biomolecular Engineering*, 2006, **23**, 213-231.
6. L. Wang and P. C. Li, *Anal Chim Acta*, 2011, **687**, 12-27.
7. G. Arrabito and B. Pignataro, *Analytical Chemistry*, 2012, **84**, 5450-5462.
8. J. A. Benn, J. Hu, B. J. Hogan, R. C. Fry, L. D. Samson and T. Thorsen, *Analytical Biochemistry*, 2006, **348**, 284-293.
9. D. S. Ginger, H. Zhang and C. A. Mirkin, *Angew Chem Int Ed Engl*, 2004, **43**, 30-45.
10. R. D. Piner, J. Zhu, F. Xu, S. Hong and C. A. Mirkin, *Science*, 1999, **283**, 661-663.
11. G. Arrabito, S. Reisewitz, L. Dehmelt, P. I. Bastiaens, B. Pignataro, H. Schroeder and C. M. Niemeyer, *Small*, 2013, **9**, 4243-4249.
12. L. M. Demers, D. S. Ginger, S. J. Park, Z. Li, S. W. Chung and C. A. Mirkin, *Science*, 2002, **296**, 1836-1838.
13. S. Li, S. Szegedi, E. Goluch and C. Liu, *Analytical Chemistry*, 2008, **80**, 5899-5904.
14. A. J. Senesi, D. I. Rozkiewicz, D. N. Reinhoudt and C. A. Mirkin, *ACS Nano*, 2009, **3**, 2394-2402.
15. H. Zhang, Z. Li and C. A. Mirkin, *Adv. Mater.*, 2002, **14**, 1472-1474.
16. E. J. Irvine, A. Hernandez-Santana, K. Faulds and D. Graham, *Analyst*, 2011, **136**, 2925-2930.
17. J. W. Jang, *Current Applied Physics*, 2014, **14**, 790-793.
18. J. Kim, Y. H. Shin, S. H. Yun, D. S. Choi, J. H. Nam, S. R. Kim, S. K. Moon, B. H. Chung, J. H. Lee, J. H. Kim, K. Y. Kim, K. M. Kim and J. H. Lim, *J Am Chem Soc*, 2012, **134**, 16500-16503.
19. S. Laing, E. J. Irvine, A. Hernandez-Santana, W. E. Smith, K. Faulds and D. Graham, *Analytical Chemistry*, 2013, **85**, 5617-5621.
20. D. G. Thompson, E. O. McKenna, A. Pitt and D. Graham, *Biosensors and Bioelectronics*, 2011, **26**, 4667-4673.
21. S. Tyagi and F. R. Kramer, *Nat Biotechnol*, 1996, **14**, 303-308.
22. C. Situma, A. J. Moehring, M. A. F. Noor and S. A. Soper, *Analytical Biochemistry*, 2007, **363**, 35-45.
23. G. Yao and W. Tan, *Analytical Biochemistry*, 2004, **331**, 216-223.
24. X. G. Dai, W. Yang, E. Firlar, S. A. E. Marras and M. Libera, *Soft Matter*, 2012, **8**, 3067-3076.
25. A. Noy, A. E. Miller, J. E. Klare, B. L. Weeks, B. W. Woods and J. J. DeYoreo, *Nano Letters*, 2002, **2**, 109-112.
26. B. Zhang, J. Zerubia and J. C. Olivo-Marin, *Appl Opt*, 2007, **46**, 1819-1829.
27. P. Krsko, M. Mansfield, S. Sukhishvili, R. Clancy and M. Libera, *Langmuir*, 2003, **19**, 5618-5625.
28. Y. Wang, E. Firlar, X. Dai and M. Libera, *Journal of Polymer Science, Part B: Polymer Physics*, 2013, **51**, 1543-1554.
29. L. Xu, A. Lio, J. Hu, D. F. Ogletree and M. Salmeron, *J Phys Chem B*, 1998, **102**, 540-548.
30. J. R. Hampton, A. A. Dameron and P. S. Weiss, *J. Am. Chem. Soc.*, 2006, **128**, 1648-1653.
31. P. Manandhar, J. Jang, G. C. Schatz, M. A. Ratner and S. Hong, *Phys Rev Lett*, 2003, **90**, 115505.
32. O. A. Nafday, M. W. Vaughn and B. L. Weeks, *J Chem Phys*, 2006, **125**, 144703.
33. P. V. Schwartz, *Langmuir*, 2002, **18**, 4041-4046.
34. G. L. Lukacs, P. Haggie, O. Seksek, D. Lechardeur, N. Freedman and A. S. Verkman, *J Biol Chem*, 2000, **275**, 1625-1629.
35. T. H. Wu, H. H. Lu and C. W. Lin, *Langmuir*, 2012, **28**, 14509-14513.
36. E. J. Peterson, B. L. Weeks, J. J. De Yoreo and P. V. Schwartz, *J Phys Chem B*, 2004, **108**, 15206-15210.
37. J. R. Hampton, A. A. Dameron and P. S. Weiss, *J Phys Chem B*, 2005, **109**, 23118-23120.
38. J. Y. Jang, S. H. Hong, G. C. Schatz and M. A. Ratner, *J. Chem. Phys.*, 2001, **115**, 2721-2729.
39. H. Wang, J. Li, H. Liu, Q. Liu, Q. Mei, Y. Wang, J. Zhu, N. He and Z. Lu, *Nucleic Acids Res.*, 2002, **30**, e61.
40. V. V. Balladur, A. Theretz and B. Mandrand, *J. Colloid. Interface. Sci.*, 1997, **194**, 408-418.